IRANIAN JOURNAL OF CATALYSIS

Experimental design study of RB 255 photocatalytic degradation under visible light using synthetic Ag/TiO_2 nanoparticles: Optimization of experimental conditions

Narges Elmi Fard[a], Reza Fazaeli[b,*]

[a]*Young Researchers and Elite Club, South Tehran Branch, Islamic Azad University, Tehran, Iran.*
[b]*Department of Chemical Engineering, Faculty of Engineering, South Tehran Branch, Islamic Azad University, Tehran, Iran.*

Received 25 September 2017; received in revised form 31 January 2018; accepted 1 February 2018

ABSTRACT

In the present study, silver-doped TiO_2 (Ag/TiO_2) nanoparticles were prepared by various Ag doping (wt%) and a combination of sol-gel and ultrasound irradiation. Ag/TiO_2 nanoparticles were characterized by energy-dispersive X-ray analysis (EDX), scanning electron microscopy (SEM) and X-ray diffraction (XRD) techniques. Based on the Taguchi method, photocatalytic degradation of (Reactive Blue 255) RB 255 azo dye was examined with Ag/TiO_2 nanoparticles under visible light irradiation. Using this method, operation factors such as Ag doping (wt%), pH, mass of catalyst (g) and RB 255 concentration (ppm) were optimized successfully. The results showed that pH, compared to the other factors, plays an important role in the photocatalytic degradation of RB 255 azo dye. The isotherm study Weber-Van Vliet and Fritz-Schlunder (IV) models are the best descriptors of equilibrium behavior. In addition, the kinetic study results indicated that the pseudo first-order has a good agreement with the experimental data.

***Keywords**: Photocatalytic degradation, Ag/TiO_2 nanoparticles, Taguchi design, RB 255.*

1. Introduction

Textile industry wastewater is one of the major sources of water pollution, which could have adverse effects on the ecosystem and environment [1,2]. Synthetic dyes are categorized as acidic, reactive, disperse, vat, metal complex, mordant, direct, basic, and sulfur dyes based on their application [3]. Reactive dyes are one of the important commercial synthetic dyes and used in the basic fabric exports in the textile industry. Also, their colors are retained under exposure to sunlight and high solubility in water [4]. RB 255 is an aromatic dye widely used in the textile industries. The azo dye is usually toxic because it is aromatic, resistant to biodegradation, carcinogenic and mutagenic properties [5-9]. The photocatalytic degradation is an effective method for treating wastewater which has been contaminated with organic and inorganic pollutants.

*Corresponding author email: r_fazaeli@azad.ac.ir
Tel./Fax: +98 21 8882 3209

In a typical method, the photocatalyst with a particular semiconductor system under visible irradiation is excited and the resultant free radicals leads to the degradation of organic pollutants. This approach has many advantages in comparison with traditional treatment techniques such as adsorption by activated carbon, chemical oxidation and biodegradation. Photocatalytic processes have many advantages for treatment of contaminated water including the complete oxidation of organic pollutants, availability of high-activity catalysts, being inexpensive and compatible with a particular design of reactor systems, and oxidizing of the pollutants in the range of micrograms per liter [10-14]. Among the semiconductor oxides, Titanium dioxide (TiO_2) has certain advantages such as stability, low cost, high photocatalytic activity, low operational temperature and low energy consumption [15]. TiO_2 has been considered a promising photocatalyst owing to its potential application in removing of all types of organic pollutants. The improvement of the photocatalytic activity of TiO_2 is

one of the most important aspects of heterogeneous photocatalysis. Attempts to increase the TiO_2 efficiency have been made by doping of a transition or noble metals [16,17]. Juang *et al*. [18] studied removal of binary azo dyes from water using UV-irradiated degradation in TiO_2 suspensions. Lai *et al*. [19] investigated TiO_2 photocatalytic degradation and transformation of oxazaphosphorine drugs in an aqueous environment. Kuo *et al*. [20] reported photocatalytic mineralization of codeine by UV-A/TiO_2 Kinetics, intermediates, and pathways. Li *et al*. [21] studied preparation of silver-modified TiO_2 via microwave-assisted method and its photocatalytic activity for toluene degradation. Lenzi *et al*. [22] investigated photocatalytic reduction of Hg (II) on TiO_2 and Ag/TiO_2 prepared by the sol–gel and impregnation methods. Angkaew and Limsuwan [23] studied preparation of silver-titanium dioxide core-shell (Ag/TiO_2) nanoparticles and effect of Ti:Ag mole ratio. García-Serrano *et al.* [24] examined the effect of Ag doping on the crystallization and phase transition of TiO_2 nanoparticles. Nalbandian *et al*. [25] carried out a research on synthesis and optimization of Ag/TiO_2 composite nanofibers for photocatalytic treatment of impaired water sources.

In this study, Ag/TiO_2 nanoparticles were synthesized and characterized. Various operation factors in removal of RB 255 using Ag/TiO_2 nanoparticles and the Taguchi method were optimized. Photocatalytic degradation of RB 255 was evaluated in terms of kinetics and thermodynamic models.

2. **Experimental**

2.1. Chemicals

Polyethylene glycol 6000 $HO(C_2H_4O)_nOH$, Titanium tetraisopropoxide (TTIP), Silver nitrate ($AgNO_3$) 99.8%, Nitric acid (HNO_3) 65% and absolute ethanol 99.8% (Merck Co., Darmshtat), RB 255 (C.I. 35945) and hydrogen peroxide (H_2O_2) 35% (Sigma-Aldrich) were purchased.

Chemical Structure of RB 255 with the molecular formula $C_{66}H_{38}C_{l2}N_{18}Na_{10}O_{34}S_{10}$ is shown Fig. 1.

2.2. Synthesis of Ag/TiO_2 nanoparticles

Ag/TiO_2 nanoparticles were prepared via ultrasonic-assisted sol-gel method. First, various amounts of $AgNO_3$ 0.019 g, 0.038 g and 0.076 g (doping Ag/TiO_2 of 0.5, 1 and 2 wt% respectively) were added into 50 mL of PEG 5% solution, then 0.1 mL acetic acid was added and the resultant mixture was stirred for 30 min (solution **I**).

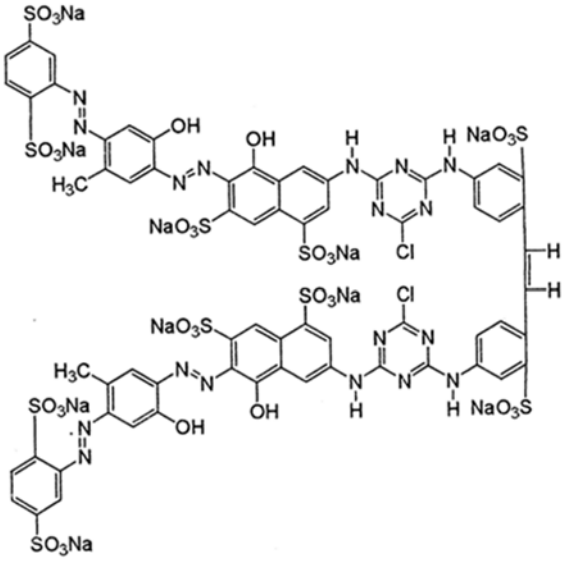

Fig. 1. Chemical Structure of RB 255.

For the next step, 8 mL of TTIP was dissolved in 40 ml absolute ethanol and stirred for 30 min to reach a homogeneous solution (solution **II**). Then, the solution **I** was added dropwise into the mixed solution **II**. The mixture was continuously stirred for 2 h, and the resultant solution was irradiated with ultrasound for 1 h. The resulting solution was stirred continuously until a gel formed for 24 h. The gel was then heated for 24 h at 80°C to evaporate the ethanol; this was followed by calcination at 550°C for 4 h and then at 650°C for 2 h to obtain the desired nanoparticles [26].

2.3. Experimental design based on the Taguchi method

The Taguchi experimental design method was introduced by Genichi Taguchi in 1960 [27,28]. This method makes it possible to determine the optimum conditions by the least number of experiments. In the Taguchi method, considering the number of selected factors and relevant levels, different orthogonal arrays as matrix experiments are used. This method presents the variability with the signal to noise (S/N) ratio [29]. The maximum S/N ratio represents the optimal experimental conditions. The orthogonal arrays are shown by Ln (XY). Where n is the number of experiments, X is the number of levels of factor and Y is the maximum number of factors which are investigated by array. **A** Taguchi orthogonal array table was used to select four effective factors. The levels and factors used in this experiment are represented in Table 1. Details of the orthogonal array L9 (34) are presented in Table 2. L is Latin square and 9 is the repetition number of the experiment. In Table 2, the numbers 1, 2, and 3 indicate the first, second, and third levels of a factor, respectively.

Table 1. Levels and factors used in this experiment.

Number of levels	Ag doping (wt%)	pH	Mass of catalyst (g)	RB 255 concentration (ppm)
1	0.5	4	0.1	100
2	1	7	0.2	200
3	2	9	0.5	300

Table 2. Taguchi design of experiments (Taguchi orthogonal array table of L_9 (3^4)).

Experiment no.	Ag doping (wt%)	pH	Mass of catalyst (g)	RB 255 concentration (ppm)
1	1	1	1	1
2	1	2	2	2
3	1	3	3	3
4	2	1	2	3
5	2	2	3	1
6	2	3	1	2
7	3	1	3	2
8	3	2	1	3
9	3	3	2	1

2.4. Reaction procedure

Various amounts of Ag/TiO_2 (0.1, 0.2 and 0.5 g), different dopant percentages (0.5, 1 and 2% (wt %)), different concentrations (100, 200 and 300 ppm) and pH levels (4, 7 and 9) were placed into the reaction vessel. 30 mL hydrogen peroxide 0.005 M was added and the suspension was stirred and irradiated by a xenon lamp for 2 h. Sampling was performed at various time intervals. The catalyst was separated by centrifuge at 9,000 rpm for 15 min. Finally, the concentration of the solution was measured at 569 nm using a UV-vis spectrophotometer. Details of all the experiments are shown in Table 3. The following formula sets out how the degradation efficiency of DR 255 was calculated.

$$\text{Degradation Efficiency}\,\% = \frac{(A_0 - A_f)}{A_0} \times 100\% \qquad \textbf{(1)}$$

A_0 is the initial and A_f is the final absorbance of the solution.

2.5. Study of reaction kinetics

0.1 g Ag/TiO_2 (0.5%) was poured into the reaction vessel. Then 160 mL Reactive Blue 255 (at different concentrations) with pH 4 and 30 ml H_2O_2 (0.005 M) was purred. The reaction mixture was irradiated under visible light. After photocatalytic degradation at different times, their absorptions were determined [30].

Table 3. Responses, S/N ratios and Means.

Experiment no.	Ag doping (wt%)	pH	Mass of catalyst (g)	RB 255 concentration (ppm)	Degradation efficiency (%)	S/N ratios (dB)	Means (dB)
1	0.5	4	0.1	100	99.99	-0.0009	0.9999
2	0.5	7	0.2	200	57.51	-4.8051	0.5751
3	0.5	9	0.5	300	27.01	-11.3695	0.2701
4	1	4	0.2	300	78.19	-2.1370	0.7819
5	1	7	0.5	100	54.57	-5.2609	0.5457
6	1	9	1	200	36.49	-8.7565	0.3649
7	2	4	0.5	200	65.52	-3.6725	0.6552
8	2	7	1	300	29.11	-10.7192	0.2911
9	2	9	2	100	21.54	-13.3351	0.2154

3. Results and Discussion

3.1. Ag/TiO_2 characterization

The XRD pattern of TiO_2 and Ag/TiO_2 nanoparticles is shown in Fig. 2. The observed diffraction pattern of TiO_2 in 2θ's (25.43), (48.28), (53.84), (55.13) and (62.07) belongs to anatase. The XRD pattern of TiO_2 are matched with the JCPDS card No. 21-1272 (anatase TiO_2). Also observed diffraction pattern of Ag/TiO_2 in 2θ's (27.52), (36.17) and (41.43) corresponds to rutile and (38.14), (44.44) and (54.41) matches with silver which is in good agreement with the standard patterns of silver (JCPDS file No. 04-0783). Between 400 to 650°C, the anatase phase changed to rutile. Growing the diffraction peaks of rutile in the samples under study showed that the presence of silver particles increased the percentage of the rutile phase.

The crystallite sizes (D) of the Ag/TiO_2 nanoparticles could also be estimated using the Debye-Scherrer [31] Eq. (2)

$$D = \frac{K\lambda}{B\cos\theta} \qquad (2)$$

where D is the crystallite size, K is the X-ray wavelength corresponding to Cu K_α radiation, λ is the cathode wavelength (nm), and B is the full width at half maximum of the highest peak. The mean particle size is calculated to be approximately 21 nm.

Fig. 3 shows SEM image of synthesized Ag/TiO_2. Bright points shows spherical silver particles, with proper distribution on the surface of the photocatalyst. The particle diameter was also measured and averaged 21 nm. The pixel count of the images was calculated using the Image Analyzer software; the percentage of area occupied by the active component of silver was estimated about 15%.

The Ag/TiO_2 elemental analysis was performed using EDX spectroscopy. The EDX spectrum of Ag/TiO_2 is shown in Fig. 4. The percentages of Ti (55.37%), O (31.48%) and Ag (12.61%) from EDX results are in good agreement with stoichiometric elemental ratios.

3.2. Design of experiments

To determine the optimum conditions, operation factors such as doped Ag (wt%), pH, mass of catalyst (g) and RB 255 concentration (ppm) were investigated. Several experiments were carried out for the design of these factors. Table 1 represents the selected levels. Response for degradation efficiency was the "bigger is better" type.

3.3. Analysis

In the standard method, the average responses method is used for statistical data analysis. Although the standard method is simple, it is not a criterium for responses distribution. Therefore, when the experiments are repeated, a precise answer can be achieved. Therefore, evaluation data distribution and the standard deviation calculation are also important. With regard to the "bigger is better" model, the higher the response value provides the lower the loss of quality.

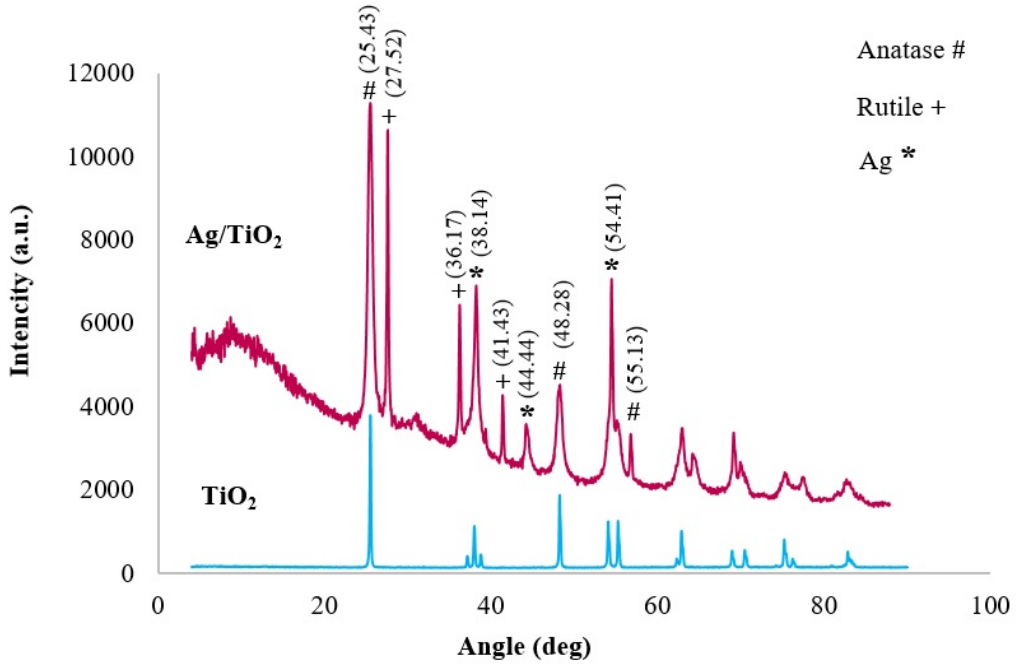

Fig. 2. X-ray diffraction pattern of TiO_2 and Ag/TiO_2 nanoparticles.

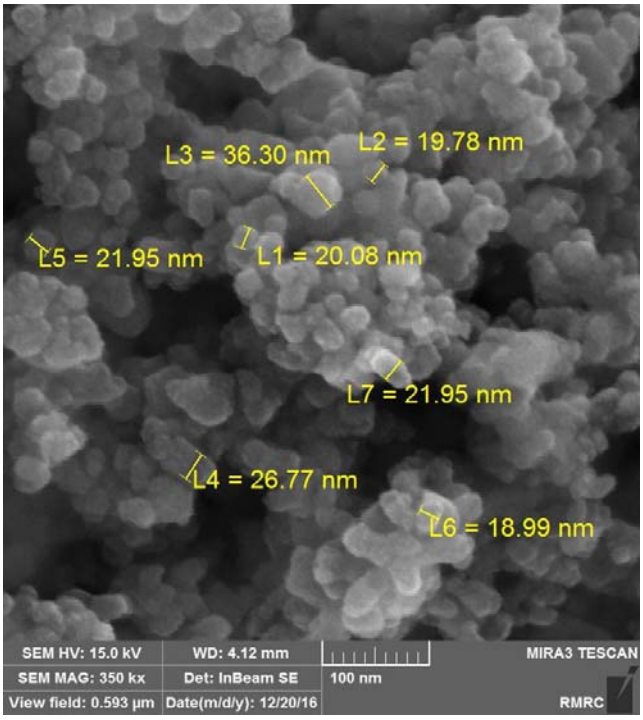

Fig. 3. SEM image of Ag/TiO_2 nanoparticles with 100 nm resolution.

Therefore, to study the response dispersion, the mean squared deviation (MSD) is calculated using Eq. (3):

$$MSD^3 = \frac{\left(\frac{1}{y_1^2} + \frac{1}{y_2^2} + \ldots + \frac{1}{y_r^2}\right)}{r} \quad (3)$$

Based on Eqs. (3) and (4), S/N ratios are calculated. In Table 3, the S/N ratios are presented.

$$\frac{S}{N} = -10 \log (MSD) \quad (4)$$

After importing data into the Minitab software Taguchi design and selection of options, the response for S/N ratios (larger is better) is shown in Table 4. Also, the response for means results are shown in Table 5. The Effects of factors are pH > Ag % > concentration of RB 255> Mass of catalyst.

Fig. 5 shows the mean of S/N ratio graph in each level factor for Ag doping, pH, mass of catalyst and RB 255 concentration. In the S/N ratios plot, each factor was put together to determine the effect of them. As can be observed in Fig. 5, based on the S/N ratio results, the difference between the minimum and maximum values belong to pH, while the least difference belongs to the mass of catalyst. According to Fig. 5, the results show that Ag doping: 0.5 wt%; pH: 4, mass of catalyst; 0.1 g and RB 255 concentration: 200 ppm with bigger S/N ratio shows the best performance. Also, a mean of means graph in each level factor of the Ag %, pH, mass of catalyst and RB 255 concentration is shown in Fig. 6.

3.4. Optimum conditions

Based on final results, the optimum conditions are Ag doping: 0.5 wt%; pH: 4, mass of catalyst: 0.1 g and RB 255 concentration: 200 ppm. To increase the accuracy, all experiments were repeated twice. The average degradation efficiency under the optimum conditions was obtained 94.46%. The results indicated that the theoretical (94.46%) and experimental (94.71%) responses are in line with the optimum conditions.

Table 4. Response for S/N ratios larger is better.

Number of levels	Ag doping (wt%)	pH	Mass of catalyst (g)	RB 255 concentration (ppm)
1	-5.392	-1.937	-6.492	-6.199
2	-5.385	-6.928	-6.759	-5.745
3	-9.242	-11.154	-6.768	-8.075
Delta	3.857	9.217	0.275	2.330
Rank	2	1	4	3

Table 5. Response for Means.

Number of levels	Ag doping (wt%)	pH	Mass of catalyst (g)	RB 255 concentration (ppm)
1	0.6150	0.8123	0.5520	0.5870
2	0.5642	0.4706	0.5241	0.5317
3	0.3872	0.2835	0.4903	0.4477
Delta	0.2278	0.5289	0.0616	0.1393
Rank	2	1	4	3

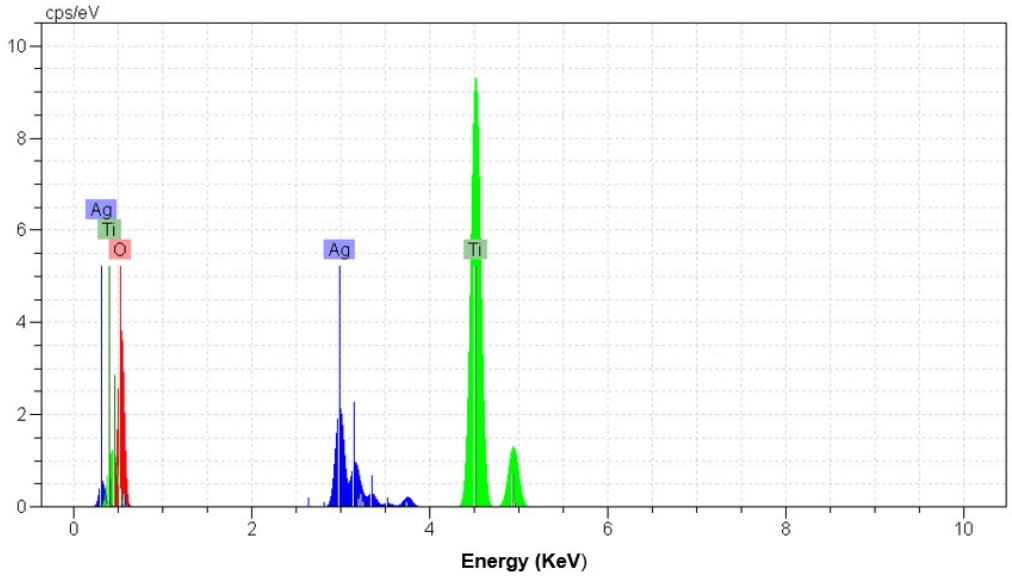

Fig. 4. Energy-dispersive X-ray analysis result of Ag/TiO_2 nanoparticles.

3.5. Effect of pH

The pH plays an important role in the rate of chemical reactions. Several experiments at different pH levels (4, 7 and 9) were carried out to study the effect of pH on RB 255 degradation. The pH changes cause a change in the photocatalytic surface charge and adsorption of azo dye molecule on the catalyst surface. The PZC of TiO_2 is around 6.8 [32].

pH > PZC: $Ag/Ti\ OH + OH^- \rightarrow Ag/TiO^- + H_2O$

pH < PZC: $Ag/Ti\ OH + H^+ \rightarrow Ag/TiOH_2$

At pH levels of less than 6.8, the surface of the catalyst was positively charged. Also, at lower pH levels, more hydroxyl radicals were produced, leading to an increase in the photocatalytic degradation rate. An increase in the pH increased the number of sites with a negative charge. Therefore, the negative sites on the catalyst surface were not effective enough to adsorb the azo dye anions. Considering pKa RB 255 (6.1), the increase pH from 4 to 9 caused the decreased photocatalytic degradation. Fig. S1 shows the effect of pH on photocatalytic degradation RB 255.

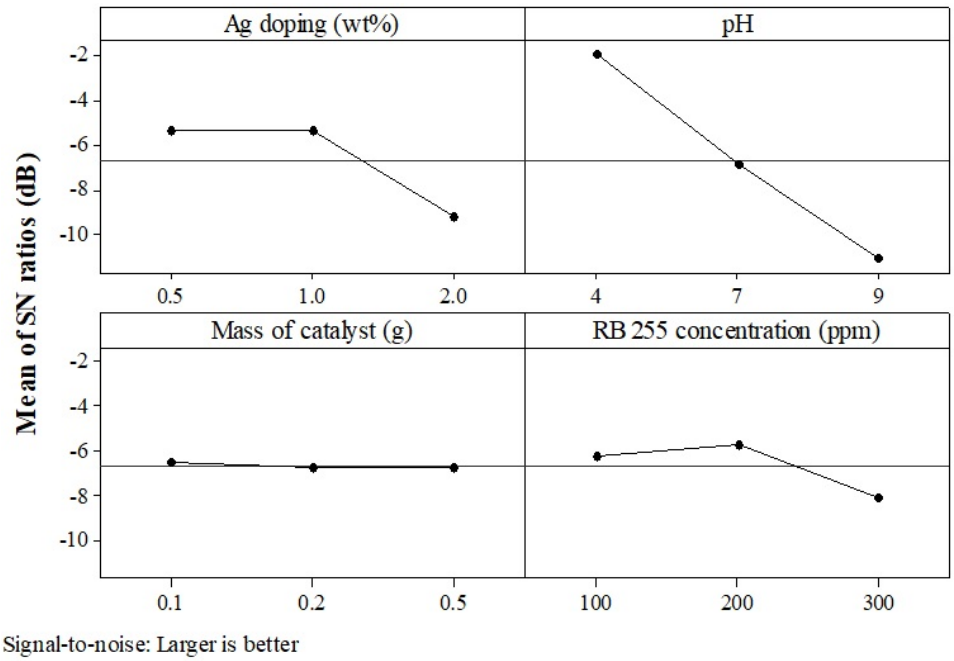

Fig. 5. S/N ratios graph for Ag doping, pH, mass of catalyst and RB 255 concentration.

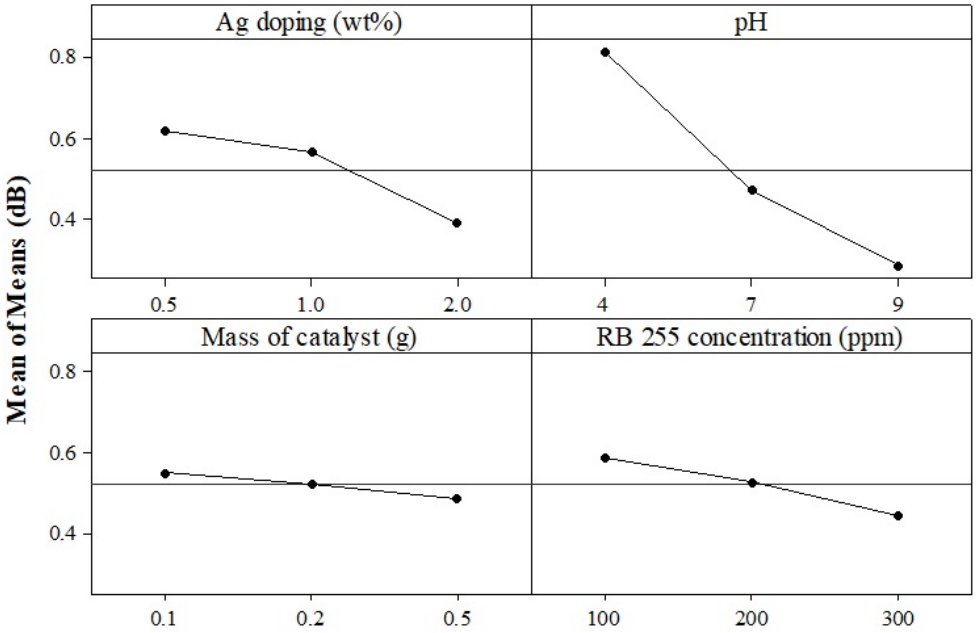

Fig. 6. Mean of means graph for Ag doping, pH, mass of catalyst and RB 255 concentration.

3.6. Effect of catalyst mass

Mass of catalyst is one of the priority variables which govern the photo removal rate of pollutant on semiconductor photocatalysis. The amount of catalyst mass affects the reaction rate, providing the sufficient surface for the adsorption and also generating oxidative valence band holes and electrons [33]. Different amounts of catalyst were examined to optimize the mass of the catalyst. The minimum amount used was 0.1 g and the maximum was 0.5 g. The results showed that increasing the mass of the catalyst enhanced the photocatalytic degradation efficiency because of the increased number of active sites. On the other hand, increasing the mass of catalyst raises the turbidity of reaction mixture and prevents light reaching the catalyst surface. Also, increasing the catalyst mass is not cost-effective. The optimum mass of catalyst obtained was 0.1 g.

3.7. Effect of Ag doping

Increasing the Ag causes the separation of electrons and cavities and improves the properties of the catalyst. The presence of doped metal ion in TiO_2 crystal affects light activity, the speed of the production of charge carriers, and the rate of electron transfer. Various amounts of $AgNO_3$ 0.019 g, 0.038 g and 0.076 g (Ag/TiO_2 doping of 0.5, 1 and 2 wt%, respectively) were examined to determine the optimal doping. The results show that increasing the active site of TiO_2 occupied with Ag decreases the surface adsorption of RB 255. Therefore, the increase of Ag amount from 0.5 to 2 decreased the photocatalytic degradation efficiency. The best value for Ag was found to be 0.5 wt%.

3.8. Effect of RB 255 concentration

Solutions with different concentrations (100, 200 and 300) of azo dye were prepared. Because of increasing the azo dye concentration in the solutions, the accessible catalyst surface to the light is restricted. At high concentrations the occupied positions on the catalyst surface by the dye molecules can limit the available active sites for photons. In addition, more photons can be absorbed by copious RB 255 molecules, leading to less photons for excitation of semiconductor present on the catalyst surface. Finally, lesser hydroxyl radicals can be produced at high RB 255 concentration leading to the decrease in decolorization efficiency [34,35]. The results show that the optimum concentration obtained was 200 ppm.

The effect of pH and Ag doping (wt %), pH and mass of catalyst (g) and pH and RB 255 concentration (ppm) on the degradation efficiency are shown in Fig. S2 (a, b, c), respectively.

Based on the results of three-dimensional graphs, pH has the most effective role in photocatalytic degradation efficiency. According to the Fig. S2 a), changing pH from 9 to 4 and Ag doping from 2 to 0.5 (wt %) simultaneously, Fig. S2 b), changing pH from 9 to 4 and mass of catalyst from 0.5 to 0.1(g) simultaneously and Fig. S2 c) changing pH from 9 to 4 and RB 255 concentration from 300 to 100 (ppm) increase photocatalytic degradation efficiency.

Also, by the contour plots, operational ranges for the affecting variable have been achieved. According to Fig. S3 (a, b, c), in the dark range (pH 4, Ag 0.5 wt %, mass of catalyst, 0.1 g and RB 255 concentration 100 ppm) degradation efficiency is higher than 90%. Also in the light range (pH 9, Ag 2 wt %, mass of catalyst, 0.5 g and RB 255 concentration 300 ppm) degradation efficiency is lower than 30%. According to these results, the pH factor has the greatest effect on the degradation efficiency.

3.9. Isothermic studies

160 mL of RB 255 solution with varying concentrations (100, 200, 300 ppm) and different pH levels (4, 7, 9) was prepared. The desired solutions were placed into the reactor's cell. 0.1, 0.2, 0.5 g Ag/TiO_2 catalyst (0.5, 1, 2 wt %), and 30 mL H_2O_2 (0.005 M) were added, then irradiated with visible light. The final concentration was measured after 120 min by UV-Visible spectrophotometer. The equilibrium adsorption capacity was obtained from equation 5:

$$q_e = \frac{(C_0 - C_e)V}{W} \quad (5)$$

3.10. Isotherm models

Experimental results have been analyzed using the models [36] shown in Table S1. A comparison of the proximity with convergence of the thermodynamic behavior of the reactions, for all the isotherm equations, was carried out using the correlation coefficient (R^2) and error functions. Because a slight difference in R^2 occurred in most fittings with the experimental data, three error functions, namely hybrid fractional error function (HYBRD) [37], Marquardt's percent standard deviation (MPSD) [38] and average relative error (ARE) [39], for the isotherms were used to choose the appropriate equation. The experimental data were fitted to the isotherm models and the statistical parameters of HYBRID, ARE and MPSD error functions were evaluated and minimized using MATLAB software. Table S2 lists the three error function equations. The error function results are shown in Tables S3, S4 and S5. Based on the results obtained from the 2, 3, and 4 parametric isotherms Tempkin, Koble Corrigan, Weber-Van Vliet and Fritz–Schlunder (IV) models with R^2 = 0989, 0.998, 0.999 and 0.999 respectively, have the lowest error values. Among all models, Weber-Van Vliet and Fritz–Schlunder (IV) models have the highest correlation and the lowest error values including HYBRID, MPSD and ARE are the best models respectively.

3.11. Kinetic models

The pseudo first-order (Langmuir-Hinshelwood and Logergren), pseudo second-order (Blanchard) and intraparticle diffusion kinetic models were used to analyze the kinetic data. A detailed description of all the kinetic models can be found in our previous study [30]. The result is shown in Table S6.

3.12. Photocatalytic degradation mechanism of azo dye

In the photocatalytic degradation process, RB 255 oxidation in the presence of hydrogen peroxide and Ag/TiO_2 catalyst was investigated under visible light irradiation. The reaction was initiated by adsorption of a photon with enough energy (equal to or higher than the band-gap). The adsorption led to a charge transfer, resulting from the transfer of electrons from the valence band to the conduction band of the semiconductor, so that the holes were generated in the valence band. Reaction between the generated holes with one reductant was generated by the oxidant products. The generated electrons reacted with water molecules and converted them into hydroxyl radicals. The mechanism of photocatalytic degradation of the azo dye by Ag/TiO_2 catalyst is as follows:

$$Ag/TiO_2 + h\upsilon \rightarrow Ag/TiO_2\left(e_{CB}^- + h_{VB}^+\right) \quad (6)$$

$$Ag/TiO_2 + \left(h_{VB}^+\right) + H_2O \rightarrow Ag/TiO_2 + H^+ + OH^\bullet \quad (7)$$

$$Ag/TiO_2 + \left(h_{VB}^+\right) + OH^- \rightarrow Ag/TiO_2 + OH^\bullet \quad (8)$$

$$Ag/TiO_2 + \left(e_{CB}^-\right) + O_2 \rightarrow Ag/TiO_2 + O_2^{\bullet -} \quad (9)$$

$$O_2^{\bullet -} + H^+ \rightarrow HO_2^\bullet \quad (10)$$

$$Dye + OH^\bullet \rightarrow \text{Degradation products} \quad (11)$$

$$Dye + h_{VB}^+ \rightarrow \text{Oxidation products} \quad (12)$$

$$Dye + e_{CB}^- \rightarrow \text{Reduction products} \quad (13)$$

4. Conclusions

Silver doped TiO_2 (Ag/TiO_2) nanoparticles were prepared by various Ag doping (wt%) and combination of sol-gel and ultrasound irradiation. The results show that Ag/TiO_2 can be easily degraded RB 255 under visible irradiation. Based on the Taguchi method, degradation efficiency was optimized. Optimized conditions with the highest efficiency was obtained at Ag: 0.5 wt%, pH:4, mass of catalyst: 0.1 g, and RB 255 concentration: 200 ppm. According to the results, pH was most effective factor for the photocatalytic degradation RB 255. The photocatalytic reaction of Ag/TiO_2 under (400-800 nm) exposure shows that the

among all models, Weber-Van Vliet and Fritz–Schlunder (IV) models which have the highest correlation and the lowest errors (HYBRID) (0.017135, 0.017639), (MPSD) (0.000093, 0.000090) and (ARE) (0.007981, 0.007880) are the best models subsequently. The kinetic results showed that the Logergren model, with the highest correlation (R^2= 0.9752) coefficient, was the best fit with the experimental data.

References

[1] S. Cheng, D.L. Oatley, P.M. Williams, C.J. Wright, Water Res. 46 (2012) 33-42.
[2] K.V. Radha, V. Sridevi, K. Kalaivani, Bioresour. Technol. 100 (2009) 987-990.
[3] A. Buthiyappan, A.R. Abdul Aziz. W.M. Ashri. W. Daud, Rev. Chem. Eng. 32 (2016) 1-47.
[4] S. Wijannarong, S. Aroonsrimorakot, P. Thavipoke, A. Kumsopa, S. Sangjan, APCBEE Proc. 5 (2013) 279-282.
[5] Q. Wang, J. Li, Y. Bai, X. Lu, Y. Ding, Sh. Yin, H. Huang, H. Ma, F. Wang, B. Su, J. Photochem. Photobiol. B 126 (2013) 47-54.
[6] A. Ehsania, R. Asgari, A. Rostami-Vartoonia, H.M. Shiri, A. Yeganeh-Faal, Iran. J. Catal. 6 (2016) 269-274.
[7] L. Vafayi, S. Gharibe, Iran. J. Catal. 5 (2015) 365-371.
[8] S. Aghdasi, M. Shokri, Iran. J. Catal. 6 (2016) 481-487.
[9] M. Karimi-Shamsabadi. M. Behpour. A. Kazemi Babaheidari. Z. Saberi, J. Photochem. Photobiol. A 346 (2017) 133-143.
[10] J. Yan, K. Wang, H. Xu, J. Qian, W. Liu, X. Yang, H. Li, Chin. J. Catal. 34 (2013) 1876-1882.
[11] L. Zhu, Z. Meng, K. Cho, W. Oh, New Carbon Mater. 27 (2012) 166-174.
[12] A.R. Khataee, M.N. Pons, O. Zahraa, J. Hazard. Mater. 168 (2009) 451-457.
[13] B. Piriti, S. Dhiraj, Sep. Purif. Technol. 85 (2012) 112-119.
[14] A. Rezaee, M.T. Ghaneian, N. Taghavinia, M.K. Aminian, S.J. Hashemian, Environ. Technol. 30 (2008) 233-239.
[15] E. Pelizzetti, Sol. Energy Mater. Sol. Cells 38 (1995) 453-457.
[16] A. Fuerte, M.D. Hernández-Alonso, A.J. Maira, A. Martínez-Arias, M. Fernández-García, J.C. Conesa, J. Soria, Chem. Commun. 24 (2001) 2718-2719.
[17] A.A. Ismail, D.W. Bahnemann, L. Robben, V. Yarovyi, M. Wark, Chem. Mater. 22 (2010) 108-116.
[18] R.S. Juang, S.H. Lin, P.Y. Hsueh, J. Hazard. Mater. 182 (2010) 820–826.
[19] W.W.P. Lai, H.H.H. Lin, A.Y.C. Lin, J. Hazard. Mater. 287 (2015) 133-141.
[20] C.S. Kuo, C.F. Lin, P.K.A. Hong, J. Hazard. Mater. 301 (2016) 137-144.
[21] X. Li, L. Wang, X. Lu, J. Hazard. Mater. 177 (2010) 639-647.
[22] G.G. Lenzi, C.V.B. Fávero, L.M.S. Colpini, H. Bernabe, M.L. Baesso, S. Specchia, O.A.A. Santos, Desalination 270 (2011) 241-247.
[23] S. Angkaew, P. Limsuwan, Procedia Eng. 32 (2012) 649-655.
[24] J. García-Serrano, E. Gómez-Hernández, M. Ocampo-Fernández, U. Pal, Curr. Appl. Phys. 9 (2009)1097-1105.
[25] M.J. Nalbandian, M. Zhang, J. Sanchez, S. Kim, Y.H. Choa, D.M. Cwiertny, N.V. Myung, J. Hazard. Mater. 299 (2015) 141-148.
[26] M. Nasir, S. Bagwasi, Y. Jiao, F. Chen, B. Tian, J. Zhang, Chem. Eng. J. 236 (2014) 388-397.
[27] G. Taguchi, Tables of orthogonal arrays and linear graphs, Maruzen, Tokyo, Japan, 1962.
[28] G. Taguchi, Introduction to Quality Engineering, Asian Productivity Organization, Tokyo, 1990.
[29] P.J. Ross, G. Taguchi, Taguchi Techniques for Quality Engineering, McGraw- Hill, New York, 1988.
[30] N. Elmi Fard, R. Fazaeli, R. Ghiasi. Chem. Eng. Technol. 39 (2016) 149-157.
[31] B.E. Warren, X-rays diffraction, Dover Publications, New York, 1990.
[32] F. Zhang, J. Zhao, T. Shen, H. Hidaka, E. Pelizzetti, N. Serpone, Appl. Catal. B 15 (1998) 147-156.
[33] M. Kilic, Z. Cinar, J. Mol. Struct. Theochem 851 (2008) 263-270.
[34] M. Guedes, J.A. Ferreira, A. Ferro, J. Colloid Interface Sci. 337 (2009) 439-448.
[35] A. Nezamzadeh-Ejhieh, A. Shirzadi, Chemosphere 107 (2014) 136-144.
[36] R. Saadi, Z. Saadi, R. Fazaeli, N. Elmi Fard. Korean J. Chem. Eng. 32. (2015) 787-799.
[37] J. Porter, G. McKay, K. Choy, Chem. Eng. Sci. 54 (1999) 5863-5885.
[38] D.W. Marquardt. J. Soc. Ind. Appl. Math. 11 (1963) 431-441.
[39] A. Kapoor, R.T. Yang, Gas Sep. Purif. 3 (1989) 187-192.